Supporting Information

Transforming Cobalt Nanospheres into Co_2P Nanorods: The Key Roles of Oleylamine and Organophosphorus Ligands in Co(I) Precursor Uncovered Through XPS Analysis

Rabah Benbalagh[1], François Rochet[1], Arthur Moisset[2], Alexandre Sodreau[3], Cassandre Bories[3], Caroline Salzemann[2], Christophe Petit[2] and Marc Petit[3]*

[1]Sorbonne Université, CNRS, Laboratoire de Chimie Physique – Matière et Rayonnement, UMR 7614, 4 place Jussieu, 75005 Paris, France

[2]Sorbonne Université, CNRS, MONARIS, UMR 8233, 4 place Jussieu, 75005 Paris, France.

[3]Sorbonne Université, CNRS, Institut Parisien de Chimie Moléculaire, UMR 8232, 75005 Paris, France.

*Corresponding author: ~~françois.rochet@sorbonne-universite.fr~~

francois.rochet@sorbonne-universite.fr

S1. Quantitative XPS

S1.1 Photoemission peak intensities and uncertainties

We give in Table S1 the photoemission peak intensities of atom X/core-level CL $I_{X\,CL}$, expressed in (counts per second)×eV, that result from peak integration after background subtraction. By multiplying $I_{X\,CL}$ by the acquisition time τ at each step (i.e. the product of the dwell-time by the number of scans), we obtain the peak area $N_{X\,CL}$. Assuming Poisson statistics, the standard deviation $\sigma_{N_{X\,CL}}$ of $N_{X\,CL}$ is $\sqrt{N_{X\,CL}}$. Thus, the relative uncertainty $\sigma_{N_{X\,CL}}/N_{X\,CL}$ is $1/\sqrt{\tau \times I_{X\,CL}}$. These values are reported in Table S2. $I_{X\,CL}$ being equal to $N_{X\,CL}/\tau$, the relative uncertainty on $I_{X\,CL}$ $\sigma_{I_{X\,CL}}/I_{X\,CL}$ is also equal to $1/\sqrt{\tau \times I_{X\,CL}}$.

Table S2 shows that $\sigma_{I_{X\,CL}}/I_{X\,CL}$ is typically 1% and never exceeds 5%.

$I_{X\,CL}$ ratios are used to calculate $\frac{I_{X\,CL}^{norm}}{I_{Y\,CL}^{norm}}$ ratios given in Table S4 after proper normalization. Other sources of inaccuracy arise from the sensitivity factors, which include the photoionization cross-section, the inelastic mean free path, and the analyzer transmission function (refer to the discussion below).

sample	$I_{Co\ 2p_{3/2}}$	$I_{Co\ 2p_{1/2}}$	$I_{Co\ 2p}$	$I_{Co\ 3p}$	$I_{Cl\ 2p}$	$I_{P\ 2s}$	$I_{P\ 2p}$	$I_{C\ 1s}$	$I_{N\ 1s}$s	$I_{O\ 1s}$
Co(II) powder	5238	3532	8770	1047	2550	1492	2041	26130	NA	3093
Co(I) powder “batch”	6132	3400	9532	1172	2822	391	714	36822	NA	5086
Co(I) diethylether-washed	23861	12000	35861	3929	5449	2027	2790	43134	NA	16864
Pure OAm	NA	NA	NA	NA	NA	NA	NA	56013	2571	8270
Aliquot 0 min 7:3 TD:OAm	1969	1176	3145	241	780	0	0	10374	654	2882
Aliquot 15 min 7:3 TD:OAm	12223	7057	19280	2482	4463	0	782	46581	3450	9900
Aliquot 30 min TD:OAm	15695	8851	24546	3398	1263	0	0	36683	2450	22212
Aliquot 45 min 7:3 TD:OAm	20522	10587	31109	6126	3913	0	0	52551	4090	10513
Aliquot 60 min 7:3 TD:OAm	11846	7082	18928	2915	5777	0	0	58334	4613	2573
9:1 TD:OAm spheres film	8748	3854	12602	2567	2062	643	NA	68925	3089	8595
9:1 TD:OAm spheres film sputtered	1888	797	2685	323	135	32	NA	5409	291	226
7:3 TD:OAm spheres film	32143	15447	47590	8903.5	2624.4	NA	2268.4	68169	3569.9	18733
7:3 spheres and rods film	13469	5336	18805	5020	1000	2407	3111	57537	2640	15284
7:3 rods film	23366	10150	33516	8808	2290	4000	5590	55536	12413	18325
7:3 rods film sputtered	197000	84580	281580	31912	2318	13756	17534	38252	3274	11318
Co Foil sputtered	197133	94641	291774	33480	0	0	0	0	0	0

Table S 1. Raw spectral intensities $I_{X\ CL}$ in (counts per second)×eV.

core-level	Co 2p		Co 3p		Cl 2p and P 2s			P 2p		C 1s		N 1s		O 1s	
sample	τ (s)	$\frac{1}{\sqrt{\tau \times I_{Co\ 2p}}}$	τ (s)	$\frac{1}{\sqrt{\tau \times I_{Co\ 3p}}}$	τ (s)	$\frac{1}{\sqrt{\tau \times I_{Cl\ 2p}}}$	$\frac{1}{\sqrt{\tau \times I_{P\ 2s}}}$	τ (s)	$\frac{1}{\sqrt{\tau \times I_{P\ 2p}}}$	τ (s)	$\frac{1}{\sqrt{\tau \times I_{C\ 1s}}}$	τ (s)	$\frac{1}{\sqrt{\tau \times I_{N\ 1s}}}$	τ (s)	$\frac{1}{\sqrt{\tau \times I_{O\ 1s}}}$
Co(II) powder	4.2	0.005	0.4	0.049	4	0.010	0.013	4	0.011	0.4	0.010			0.4	0.028
Co(I) powder "batch"	4	0.005	4	0.015	4.5	0.009	0.024	4.5	0.018	3.5	0.003			3.5	0.007
Co(I) diethylether washed	4	0.003	3	0.009	4	0.007	0.011	4	0.009	1	0.005			2	0.005
Pure OAm										1	0.004	2.5	0.012		
Aliquot 0 min 7:3 TD:Oam	10	0.006	10	0.020	5	0.016	-	10	-	1.5	0.008	10	0.012	2.5	0.012
Aliquot 15 min 7:3 TD:Oam	3	0.004	2	0.014	4	0.007	-	4	-	1	0.005	2.5	0.011	1	0.010
Aliquot 30 min 7:3 TD:Oam	10	0.002	10	0.005	36	0.005	-	23	-	1.5	0.004	5	0.009	2.5	0.004
Aliquot 45 min 7:3 TD:Oam	2.5	0.004	2	0.009	2	0.011	-	2	-	1	0.004	2.5	0.010	1	0.010
Aliquot 60 min 7:3 TD:Oam	1.5	0.006	1.5	0.015	1.5	0.011	-	1.5	-	1	0.004	2.5	0.009	1	0.020
9:1 TD:Oam spheres film	1.8	0.007	1.6	0.016	5	0.010	0.018		-	0.4	0.006	8.4	0.006	0.4	0.017
9:1 TD:Oam spheres film sputtered	1.5	0.016	2	0.039	2.5	0.054	0.112		-	1	0.014	6	0.024	2	0.047
7:3 TD:Oam spheres film	0.5	0.006	1	0.011	4	0.010	-	4	0.010	1	0.004	4	0.008	0.5	0.010
7:3 TD:Oam spheres and rods film	1	0.007	0.5	0.020	2.5	0.020	0.013	2.5	0.011	0.5	0.006	2.5	0.012	0.5	0.011
7:3 TD:Oam rods film	0.2	0.012	0.2	0.024	0.2	0.047	0.035	0.2	0.030	0.05	0.019	0.2	0.020	0.2	0.017
7:3 TD:Oam rods film sputtered	0.6	0.002	0.6	0.007	0.4	0.033	0.013	0.4	0.012	0.6	0.007	1	0.017	1	0.009
Co Foil sputtered	0.2	0.004	0.3	0.010											

Table S2. Acquisition time τ (dwell-time $\times$ number of scans) and $1/\sqrt{\tau \times I_{X\,CL}}$ values ($I_{X\,CL}$ values are from Table S1). It corresponds to the relative uncertainties $\sigma_{N_{X\,CL}}/N_{X\,CL}$ where $N_{X\,CL}$ is the number of counts $\times$ eV and $\sigma_{I_{X\,CL}}/I_{X\,CL}$ assuming Poisson statistics.

S1.2 Inelastic mean free paths λ

Inelastic mean free paths λ depend on the kinetic energy (KE) of the photoelectrons and on the material. λ were calculated for oleylamine using the TPP-2M equation,[1–5,6] with a density ρ of 0.813 g×cm^{-3}, and a number of valence electron N_V of 114. As the optical band gap E_g of OAm is not available, we took 3 eV, which is a typical value for linear and cyclic alkane chains.[7] For TD, we used ρ=0.759 g×cm^{-3}, N_V=86, and E_g=3 eV. The λ values of OAm and TD are equal to 0.5 %. With the TPP-2M equation, we also calculated the λ for bulk Co, Co_2P (metallic, N_V=23, ρ=7.66 g.cm^{-3}), CoP (metallic, N_V=14, ρ==6.48 g.cm^{-3}). Calculated λ are plotted in Figure S1.

In the 706-1436 eV range TPP-2M λ can be simply fitted by a power law of the kinetic energy (*KE*):

$$\lambda(KE) = A \times KE^{\alpha} \qquad \textit{Equation S1}$$

where A is a constant, see Figure S1. Both parameters A and α are let free for Co and OAm/TD. The exponent α depends on the material: it is 0.741 for Co and 0.801 for OAm/TD.

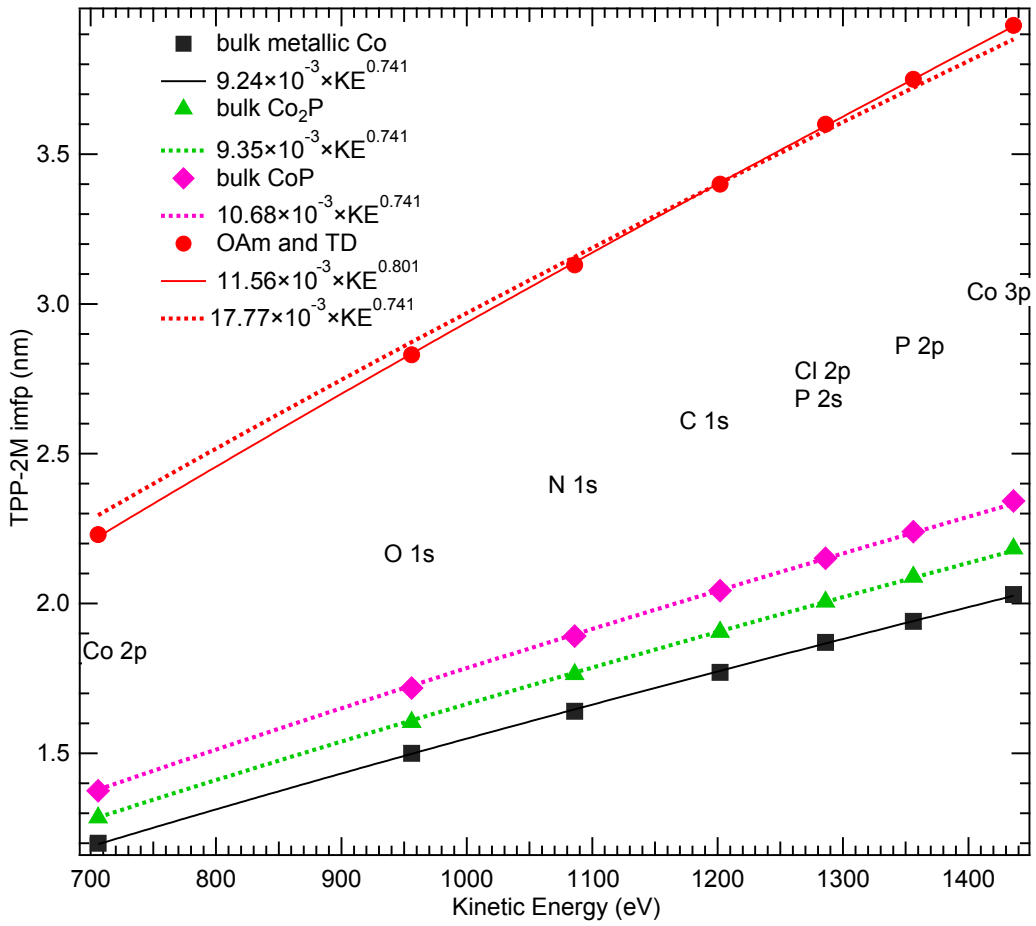

Figure S1. (TPP-2M λ values in bulk cobalt (black squares), bulk Co2P (green triangles), bulk CoP (pink diamonds) and OAm/TD (red disks) in the 706-1436 eV energy interval. Solid lines: power law best fits with two free parameters A and α ($\lambda = A \times KE^{\alpha}$). For Co_2P, CoP and OAm/TD λ values, the dotted line is a fit using the same exponent (α=0.741) as that found for bulk Co.

However, the difference is small. Taking for OAm/TD the same α value of 0.741 than for Co (the red dotted line is the fit of OAm/TD λ with α fixed at 0.741), the maximum error on the TPP-2M λ is 2.8% at 706 eV (note that the precision on TPP-2M λ is estimated to be ±11%[4,8]). For Co_2P and CoP, α fixed at 0.741 gives excellent fits of the TPP-2M λ's (note that the λ curves of Co_2P and CoP are nearly parallel to that of Co, with small offsets of +0.12 nm and +0.24 nm for Co_2P and CoP, respectively).

S1.3 Normalization procedures of the raw photoemission intensities

Considering that the geometry, slit widths, pass energy (and hence analyzer transmission factor), and detector yield are all kept constant during the measurements, then the intensity of the atom X core-level (CL) peak is:

$$I_{X\,CL} = K \times n_{Co}^{medium} \times \sigma_{XCL} \times T_{lens} \times \lambda_{X\,CL}^{medium} \qquad \textit{Equation S2}$$

where K is a constant, n_{Co}^{medium} the number of X atoms per unit volume, σ_{XCL} the atom X CL photoionization cross-section (that depends on hν, fixed here, taken from ref [9]), T_{lens} *the lens transmission factor, and* $\lambda_{X\,CL}$ the *inelastic mean free path* of a photoelectron emitted from the atom X CL with kinetic energy KE. Asymmetry parameters are irrelevant as the measurements are made at magic angle.

Under the crucial assumption that n_{Co}^{medium} is constant with depth *z* for a given sample, then the core-level intensity can be normalized by dividing it by the quantity $\sigma_{XCL} \times T_{lens} \times \lambda_{X\,CL}^{medium}$.

$$I_{X\,CL}^{norm} = \frac{I_{X\,CL}}{\sigma_{XCL} \times T_{lens} \times \lambda_{X\,CL}^{medium}} \qquad \textit{Equation S3}$$

We have already seen that $\lambda_{X\,CL}^{medium}$ can be approximated by a power function of KE

$$\lambda(KE) = A \times KE^{\alpha} \qquad \textit{Equation S4}$$

As T_{lens} is a power function of KE ($T_{lens} = B \times (KE)^{\beta}$ ($\beta < 0$)), the product $T_{lens} \times \lambda_{X\,CL}$ is also a power function of KE ($\propto (KE)^{\alpha+\beta}$).

Consequently, the normalized core-level intensities I_X^{norm} writes as:

$$I_{X\,CL}^{norm} = \frac{I_X}{Q_{X\,CL}} \qquad \textit{Equation S5}$$

with $Q_{X\,CL} = \sigma_{X\,CL} \times (KE)^{\alpha+\beta}$, i.e. the sensitivity factor.

The value of $\alpha + \beta$ can be obtained considering that the ratio $\frac{I_{Co\,3p}^{norm}}{I_{Co\,2p}^{norm}}$ of the cleaned Co foil (a sample that is homogeneous in-depth) is necessarily equal to one, taking α fixed at 0.741 (all λ's follow a "universal" law $\propto(KE)^{0.741}$ which is reasonable one in view of the fits of the TPP-2M λ of metallic cobalt and OAm (Figure S1(a)). The main source of inaccuracy lies in background subtraction and peak area measurement. Moreover, Co LMM Auger can contribute to Co $2p_{3/2}$ intensity. β is found equal to -0.571, -0.514, and -0.552 using the Co $2p_{3/2}$; Co $2p_{1/2}$ and overall Co 2p areas, respectively. The sensitivity factors $Q_{X\,CL}$ are given in Table S2 of the SI. In practice, we will adopt $Q_{X\,CL}$ values calculated with the overall Co 2p intensity.

Equation S5, *only valid for in-depth homogeneous samples,* can be applied to *all* measured core-level intensities, *whatever* the material (powder, aliquots, concentrated particle films). Naturally, for $\frac{I_{Co\,3p}^{norm}}{I_{Co\,2p}^{norm}}$ plotted in Figure S2, any departure from one is indicative of in-depth inhomogeneity. Complex powders and aliquots taken between 0 and 30 min $\frac{I_{Co\,3p}^{norm}}{I_{Co\,2p}^{norm}}$ values equal to 1 ± 0.2. However when the particles in the TD:OAm mixture reach a size of 6 nm or bigger (45 min and 60 min), then $\frac{I_{Co\,3p}^{norm}}{I_{Co\,2p}^{norm}}$ is notably greater than 1 ($1.4 - 1.7$). This is also particularly clear for the centrifugated, washed particle films that are highly inhomogeneous and for which $\frac{I_{Co\,3p}^{norm}}{I_{Co\,2p}^{norm}} \sim 1.8 - 2.4$.

CL	$\sigma_{X\,CL}$ (Mbarn)	KE (eV)	Calibration Co $2p_{3/2}$ $\beta = -0.57097$	Calibration Co $2p_{1/2}$ $\beta = -0.51373$	Calibration Co 2p $\beta = -0.55215$
			$Q_{X\,CL}$	$Q_{X\,CL}$	$Q_{X\,CL}$
Co 2p	0.25910	706	0.79041	1.15058	0.89428126
O 1s	0.04005	956	0.12864	0.19053	0.14637685
N 1s	0.02451	1086	0.08045	0.12003	0.09176359
C 1s	0.01367	1202	0.04565	0.06851	0.05216981
Cl 2p	0.03103	1286	0.10482	0.15791	0.11994242
P 2s	0.01603	1286	0.05415	0.08158	0.06196187
P 2p	0.01621	1356	0.05525	0.08349	0.06328797
Co 3p	0.02600	1436	0.08949	0.13568	0.10261551

Table S3. Sensitivity factor $Q_{X\,CL} = \sigma_{X\,CL} \times (KE)^{\alpha + \beta}$ *calculated with* α*=0.741 and* β *values deduced from the Co* $2p_{3/2}$*, Co* $2p_{1/2}$ *and Co 2p intensities of the clean cobalt foil (see main paper).*

sample	$\frac{I^{norm}_{Co\ 3p}}{I^{norm}_{Co\ 2p}}$	$\frac{I^{norm}_{P\ 2s}}{I^{norm}_{P\ 2p}}$	$\frac{I^{norm}_{Cl\ 2p}}{I^{norm}_{Co\ 2p}}$	$\frac{I^{norm}_{Cl\ 2p}}{I^{norm}_{Co\ 3p}}$	$\frac{I^{norm}_{P\ 2s}}{I^{norm}_{Co\ 2p}}$	$\frac{I^{norm}_{P\ 2p}}{I^{norm}_{Co\ 2p}}$	$\frac{I^{norm}_{P\ 2s}}{I^{norm}_{Co\ 3p}}$	$\frac{I^{norm}_{P\ 2p}}{I^{norm}_{Co\ 3p}}$	$\frac{I^{norm}_{N\ 1s}}{I^{norm}_{Co\ 2p}}$	$\frac{I^{norm}_{N\ 1s}}{I^{norm}_{Co\ 3p}}$	$\frac{I^{norm}_{C\ 1s}}{I^{norm}_{P\ 2p}}$	$\frac{I^{norm}_{C\ 1s}}{I^{norm}_{P\ 2s}}$	$\frac{I^{norm}_{O\ 1s}}{I^{norm}_{Co\ 2p}}$	$\frac{I^{norm}_{C\ 1s}}{I^{norm}_{N\ 1s}}$
Co(II) powder	1.04	0.75	2.17	2.08	2.46	3.29	2.36	3.16	NA	NA	15.53	20.80	2.15	NA
Co(I) batch	1.07	0.56	2.2	2.1	0.60	1.05	0.60	1.00	NA	NA	-	-	3.2	NA
Co(I) washed diethylether	0.95	0.74	1.1	1.2	0.82	1.1	0.85	1.1	NA	NA	18.7	25	2.9	NA
Pure OAm	NA	NA	NA	NA	NA	NA	NA	NA	NA	NA	NA	NA	NA	38
Aliquot 0 min 7:3 TD:OAm	0.7	NA	1.8	2.8	0	0	0	0	2.02	3.03	NA	NA	5.6	28
Aliquot 15 min 7:3 TD:OAm	1.1	NA	1.73	1.54	0.00	0.00	0.00	NA	1.74	1.55	NA	NA	3.14	24
Aliquot 30 min 7:3 TD:OAm	1.2	NA	0.4	0.3	0	0	0	0	0.97	0.81	NA	NA	5.5	26
Aliquot 45 min 7:3 TD:OAm	1.7	NA	0.94	0.55	0.00	0.00	0.00	NA	1.28	0.75	NA	NA	2.06	23
Aliquot 60 min 7:3 TD:OAm	1.3	NA	2.28	1.70	0.00	0.00	0.00	NA	2.38	1.77	NA	NA	0.83	22
9:1 TD:OAm spheres film	1.78	NA	1.22	0.69	0.74	NA	0.41	NA	2.39	1.35	NA	127.31	4.17	39
9:1 TD:OAm spheres film sputtered	1.05	NA	0.37	0.36	0.17	NA	0.16	NA	1.06	1.01	NA	200.76	0.51	33
7:3 TD:OAm spheres film	1.63	NA	0.41	0.25	NA	0.67	NA	0.41	0.73	0.45	36.46	NA	2.40	34
7:3 spheres and rods film	2.33	0.79	0.40	0.17	1.85	2.34	0.79	1.00	1.37	0.59	22.44	28.39	4.97	38
7:3 rods film	2.17	0.73	0.48	0.22	1.63	2.23	0.75	1.03	3.42	1.60	12.1	16.5	3.17	8
7:3 rods film sputtered	0.99	0.80	0.06	0.06	0.71	0.88	0.71	0.89	0.11	0.11	2.65	3.30	0.25	20
Co Foil sputtered	1.00	NA	NA	NA	NA	NA	NA	NA	NA	NA	NA	NA	NA	NA

Table S4. Useful $\frac{I^{norm}_{X\ CL}}{I^{norm}_{Y\ CL}}$ *ratios.*

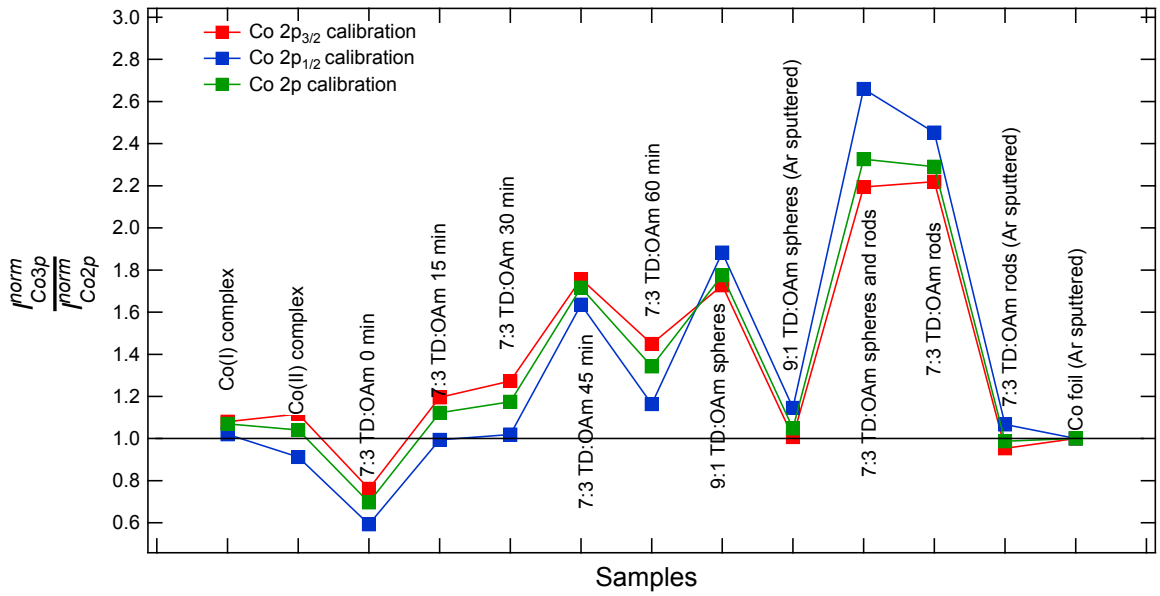

Figure S2. $\frac{I^{norm}_{Co\ 3p}}{I^{norm}_{Co\ 2p}}$ *for the various samples examined in this study. Any strong departure from one is indicative of the sample in-depth inhomogeneity. The clean Co foil (a homogeneous sample with* n_{Co} *constant with depth) was used to determine the lens transmission* $T_{lens} \propto KE^{-\beta}$ *for which* β *was-0.571, -0.514 and -0.552 when the Co* $2p_{3/2}$*, Co* $2p_{1/2}$ *and total Co 2p areas were used, respectively.*

S1.4 Quantitative XPS analysis of the Co(II)Cl2(PPh_3*)*$_2$ *and Co(I)ClP*Ph_3 *powders*

Figure S2 shows that $\frac{I^{norm}_{Co\ 3p}}{I^{norm}_{Co\ 2p}}$ is 1.04 for the Co(II) powder, 1.07 for the "batch" Co(I) powder, and 0.95 after washing of the latter in diethylether. A deviation of less than 10% is indicative that cobalt atoms are homogeneously distributed in the depth of the samples. *Assuming that chlorine and phosphorus atoms are also homogeneously distributed in the materials,* the $\frac{I^{norm}_{X\ CL}}{I^{norm}_{Y\ CL}}$ ratios yield atomic ratios $\frac{[X]}{[Y]}$ that can be compared with nominal stoichiometries.

For the nominal Co(II)$Cl_2(PPh_3)_2$ powder, $\frac{[Cl]}{[Co]}$ is ~2.2 (close to 2, the ratio expected from the oxidation state of cobalt). $\frac{[P]}{[Co]}$ ratio is ~2.8, greater than the expected value of 2. This may be due to an excess of phosphine used in the formation of Co(II)$Cl_2(P(C_5H_6)_3)_2$ from $CoCl_2 \cdot 6H_2O$. For its part, $\frac{[C]}{[P]}$ ratio is in the 16-21 range, in good accord with the stoichiometry of triphenylphosphine ($P(C_6H_5)_3$).

While elemental "bulk" macroscopic analysis of both the 'batch" and washed Co(I) powders is in accordance with the nominal stoichiometry, quantitative XPS analysis provides conflicting results. For the Co(I) "batch" powder, $\frac{[Cl]}{[Co]}$ is ~2, which contrasts with the expected stoichiometric ratio of 1. After washing the powder in diethylether $\frac{[Cl]}{[Co]}$ is ~1, this time in very good agreement with the stoichiometry. Apparently washing eliminates the excess of chloride. According to the nominal stoichiometry, the $\frac{[P]}{[Co]}$ ratio should be 3. In fact, the measured one is much smaller, 1.1 for the "batch", and 0.8 for the diethylether-washed powder. $\frac{[C]}{[P]}$ is in the 19-25 range for the diethylether-washed sample, which is in satisfactory accord with the expected ratio of 18. The reason for the discrepancies between macroscopic analysis and XPS may be attributed to the surface sensitivity of the latter technique (λ ranges from ~2 to ~4 nm for the core-level photoelectrons analyzed in this study). The surface composition of the macroscopic grains constituting the powder may differ from that of the bulk.

S2. Core level spectra of diamagnetic $HCo(I)[PhP(OEt)_2]_4$ and $HCo(I)[P(OPh)_3]_4$ complexes

The ligand structure of $HCo(I)[PhP(OEt)_2]_4$ is roughly trigonal bipyramidal,[10] with the P atoms in a tetrahedral configuration. Data on $HCo(I)[P(OPh)_3]_4$ is lacking. However, the X-ray crystal structure of $HCo(I)[P(OEt)_3]_4$ shows also that the 4 P atoms are in a distorted tetrahedral configuration, and considering the H atom the configuration about each cobalt atom is roughly trigonal bipyramidal.[11] Co(I) complexes that have trigonal bipyramidal geometry are diamagnetic (S=0).[12] The XPS spectra of these zero spin complexes are shown in Figure S3. Due to charging, the flood gun is used.

The C 1s (Figure S3(a)) of the organophosphorus ligands presents two components, one due to C-C bonds (fixed at 285 eV), and one shifted by 1.5 eV, due to C-O bonds. The (C-O):(C-C) component distribution is 1:5 and 1:4 for the phosphite (in $HCo(P(OPh)_3)_4$) and the phosphonite (in $HCo(PhP(OEt)_2)_4$) powders, respectively. We note that the spectral weight of the C-O component is greater in the C 1s spectrum of $HCo(PhP(OEt)_2)_4$ than in that of $HCo(P(OPh)_3)_4$. Note that the other spectra (P 2p, Co 2p) will be aligned in binding energy with respect to the C-C component fixed at 285 eV.

The P 2p spectra are shown in Figure S3(b). That of the phosphite in $HCo(P(OPh)_3)_4$ is fitted with a single doublet, with P $2p_{3/2}$ at 133.3 eV. In contrast, the P 2p spectrum of the phosphonite in $HCo(PhP(OEt)_2)_4$ is fitted with two doublets, the major one with P $2p_{3/2}$ at 132.0 eV, and a minor, one with P $2p_{3/2}$ at 132.1 eV. The binding energy shift of +1.3 eV observed between the phosphonite (main peak) and the phosphite doublet is easily understandable as due to an increased charge transfer associated to an increased number of oxygen neighbors around P, from 2 in the phosphonite to 3 in the phosphite. The BE of the minor, red-shaded doublet in the $HCo(PhP(OEt)_2)_4$ P 2p spectrum nearly coincides with that of the phosphite.

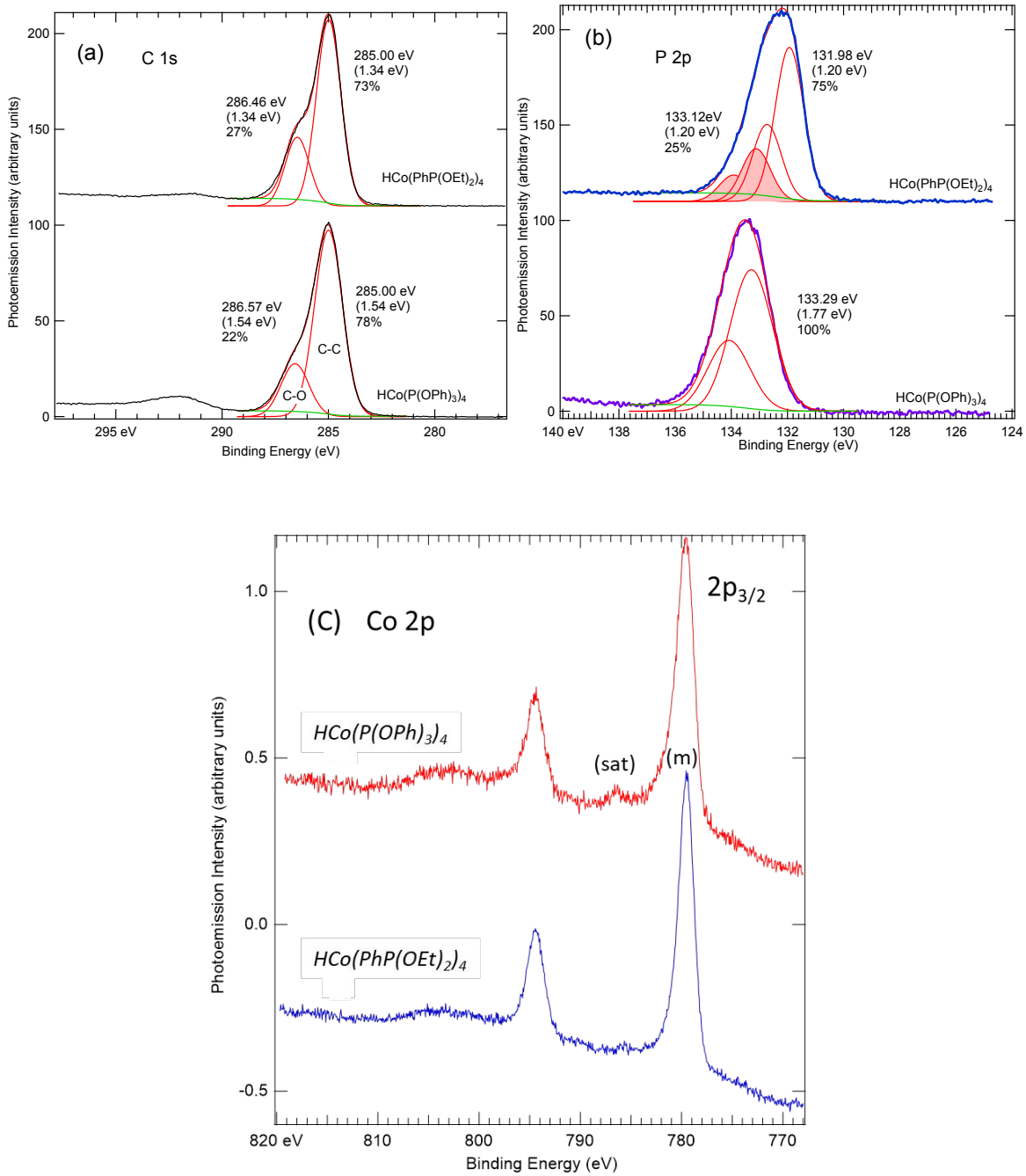

Figure S3. (a) C 1s, (b) P 2p and (c) Co 2p spectra of $HCo(P(OPh)_3)_4$ and $HCo(PhP(OEt)_2)_4$. BE are referenced to the C 1s peak (C-C bond) positioned at 285.0 eV. C 1s and P $2p_{3/2}$ BE, FWHM (between parentheses) and spectral weights are indicated. A monochromatized AlK_α source (1486.71 eV) was used.

This strongly suggests that $PhP(OEt)_2$ is oxidized to phosphite $P(OPh)P(OEt)_2$. A phosphate $O=P(OPh)P(OEt)_2$ is excluded as its BE should be ~134.5 eV.[13] We attribute this oxidation to a reaction of $HCo(I)(PhP(OEt)_2)_4$ with O_2 during exposure to air. As discussed in the main paper, a peroxo $HCo(PhP(OEt)_2)_4O_2$ intermediate (formally Co(III)) is formed which then decomposes to give $P(OPh)P(OEt)_2$. Note that the maximum number of oxygen atoms around phosphorus is 3. The phosphite ligand cannot transform into a phosphate (a O=P bond does not form). More generally, this observation emphasizes the capacity of the Co(I) complexes to catalyze the oxidation of the organophosphorus ligands, as also discussed for $Co(I)Cl(PPh_3)_3$ in the main paper.

The Co 2p spectra are shown in Figure S3(c). For both complexes, we observe a single strong Co $2p_{3/2}$ peak at ~780 eV. A weak component at 785 eV is also seen, in contrast to the case of the high spin tetrahedral $Co(I)Cl(PPh_3)_3$ which exhibited a strong satellite. The narrowness of the main peak suggests the absence of spin multiplet, and thus no spin interaction between the $2p^5$ and the valence band which can be understood if in the final state the 3d occupation remains $3d^8$ with S=0.

S3. N 1s spectra of the TD:OAm aliquots

The N 1s spectra 1s of the precursor-containing 7:3 TD:OAm mixture aliquots are given in Figure S4. Note that the peaks are symmetric, which means that differential charging is correctly addressed with the flood. The average BE is 399.6±0.3 eV, a typical value for an amine. There are no indication of ammonium, C=N or C≡N contributions.[14]

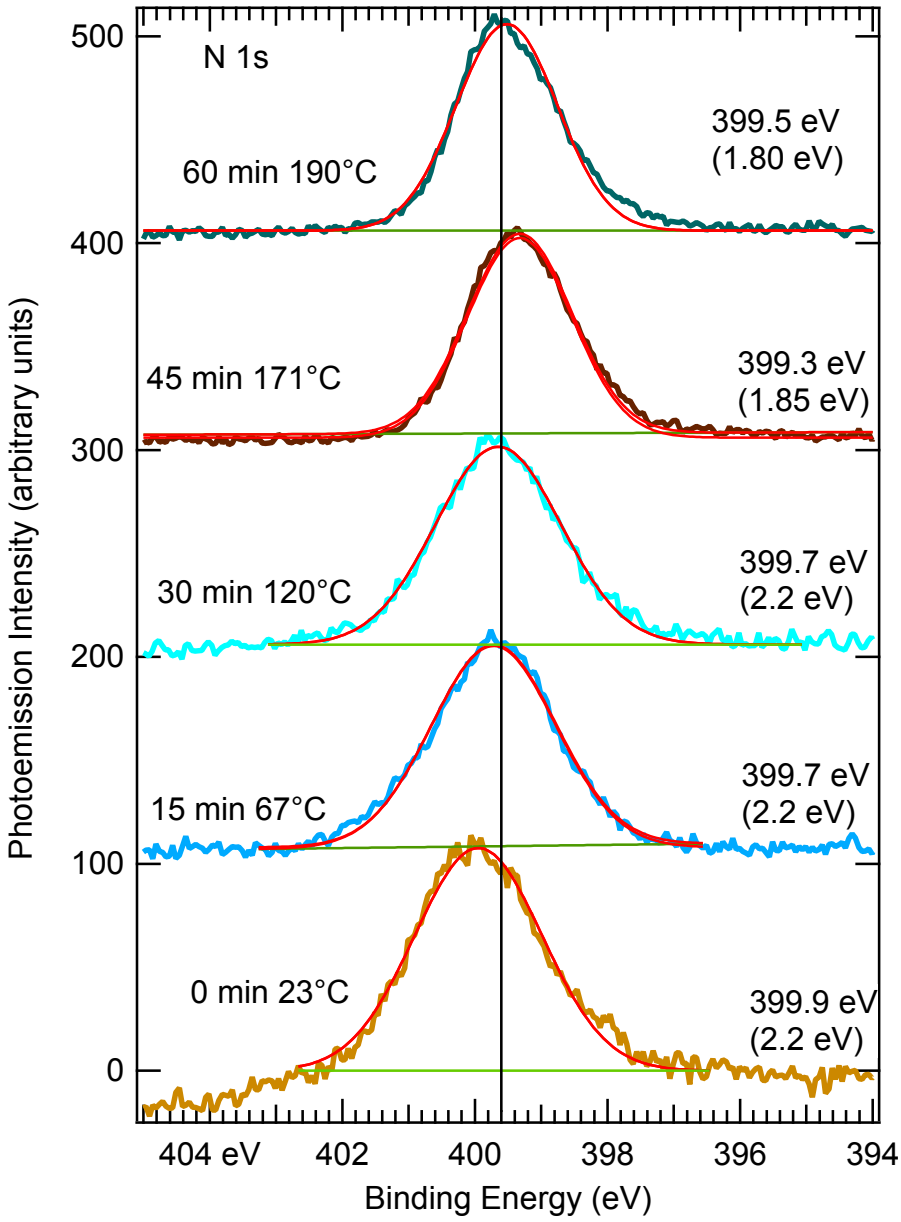

Figure S4. N 1s core-levels of the precursor-containing 7:3 TD:OAm mixture aliquots. The spectra are fitted with a single Gaussian whose position and FWHM (between parentheses) are indicated. All BE are referenced to the C 1s peak positioned at 285 eV. The average oleylamine BE is then 399.6±0.3 eV. A monochromatized Al K_α source (1486.71 eV) was used.

S4. $\frac{I_{C\,1s}^{norm}}{I_{N\,1s}^{norm}}$ for pure OAm, 7:3 TD:OAm mixture and the concentrated washed particle films

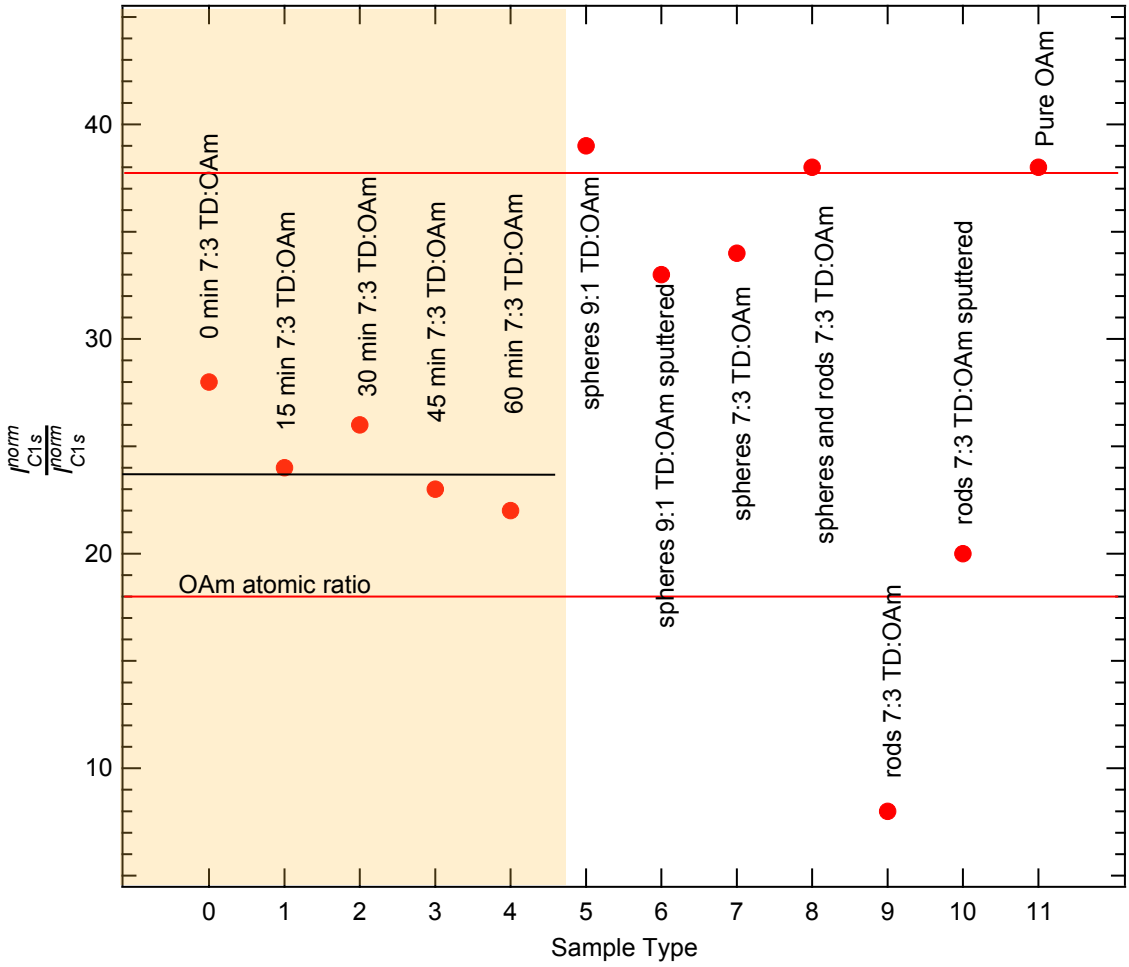

Figure S5. $\frac{I_{C\,1s}^{norm}}{I_{N\,1s}^{norm}}$ *for the 7:3 TD:OAm mixture and for the concentrated washed particle films.*

Pure OAm ($C_{18}H_{37}N$) has a C/N ratio of 18. A 7:3 TD:OAm mixture has a C/N ratio of 59.

S5. Particles grown in THF at room temperature

Co nanoparticles are prepared from the Co(I) precursor in tetrahydrofuran (THF). Tetrahydrofuran (THF) is distillated under nitrogen then dried over molecular sieves 4Å (Sigma-Aldrich) and finally degassed by Argon. The synthesis is made *at room temperature* (5-6 min) according to the disproportionation reaction:

$$2CoCl(PPh_3)_3 \rightarrow CoCl_2(PPh_3)_2 + Co + 4\ PPh_3$$

In the absence of the OAm ligand, the nanoparticles of size ~ 10 nm tend to cluster, as shown in Figure S6.

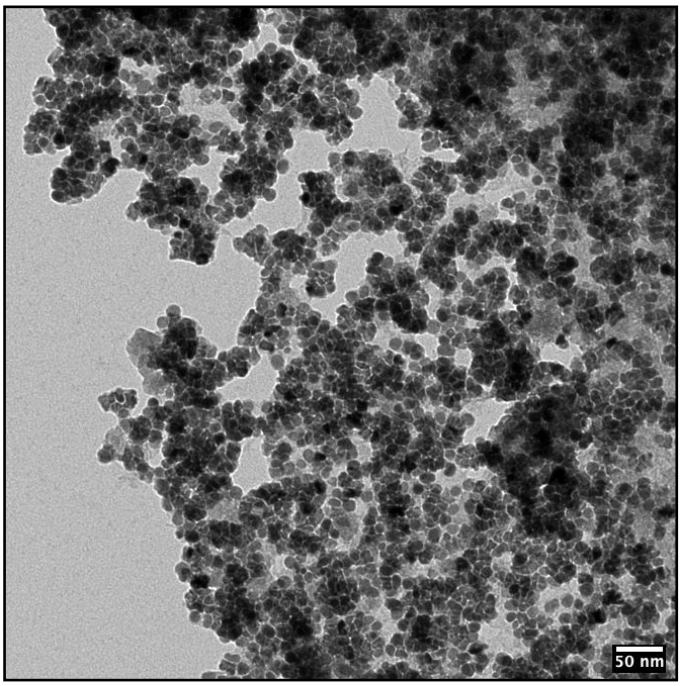

Figure S6. TEM micrographs of the solid part obtained after washing and centrifugation. The spheres were grown at room temperature in THF solution.

The Co 2p spectrum shown in Figure S7 shows that the metallic particles (metal: Co $2p_{3/2}$ peak at 778 eV) are heavily oxidized (oxide: Co $2p_{3/2}$ main peak at 781 eV, and satellite at ~786 eV).

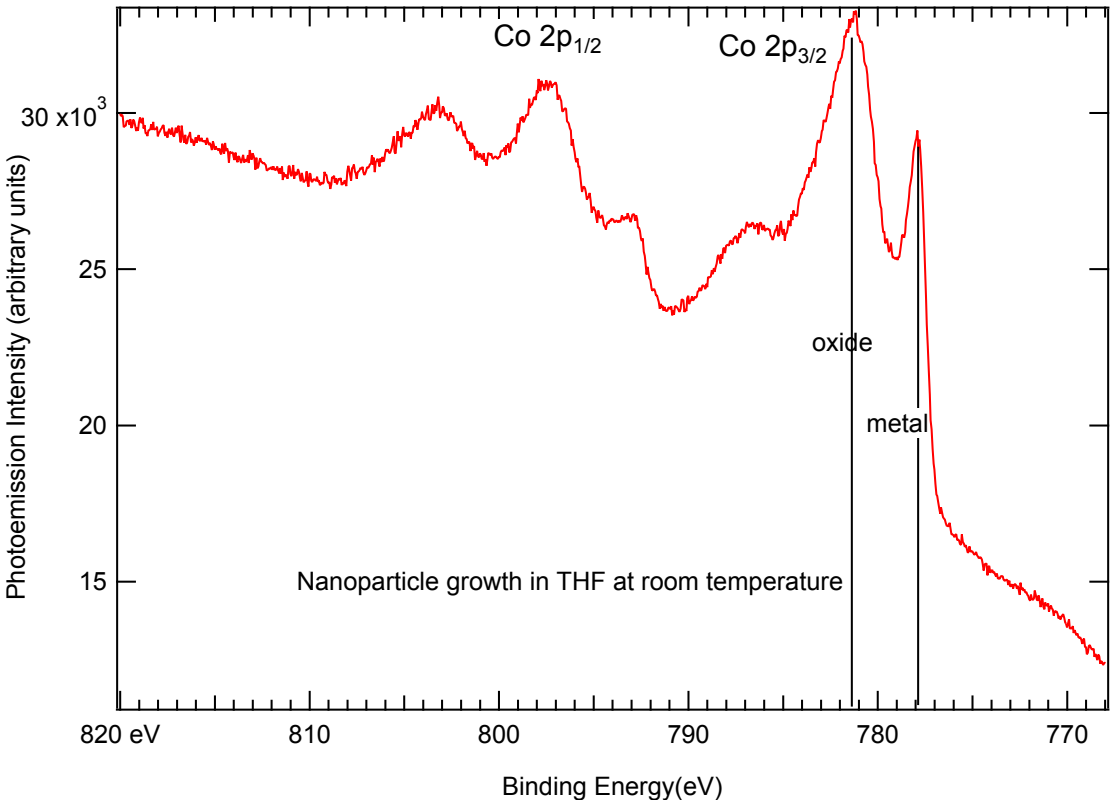

Figure S7. Co 2p spectra of concentrated nanoparticles (spheres) grown at room temperature in THF. BE are referenced to C 1s positioned at 285.0 eV. A monochromatized Al K_α source (1486.71 eV) was used.

The corresponding Cl 2p/P 2s spectral region is shown in Figure S8. The P 2s region does not allow the observation of phosphorus species. Most phosphorus species are likely washed out during the preparation of the concentrated particle film. PPh_3 should be peaked at 190-191 eV and Co_2P at 187 eV.

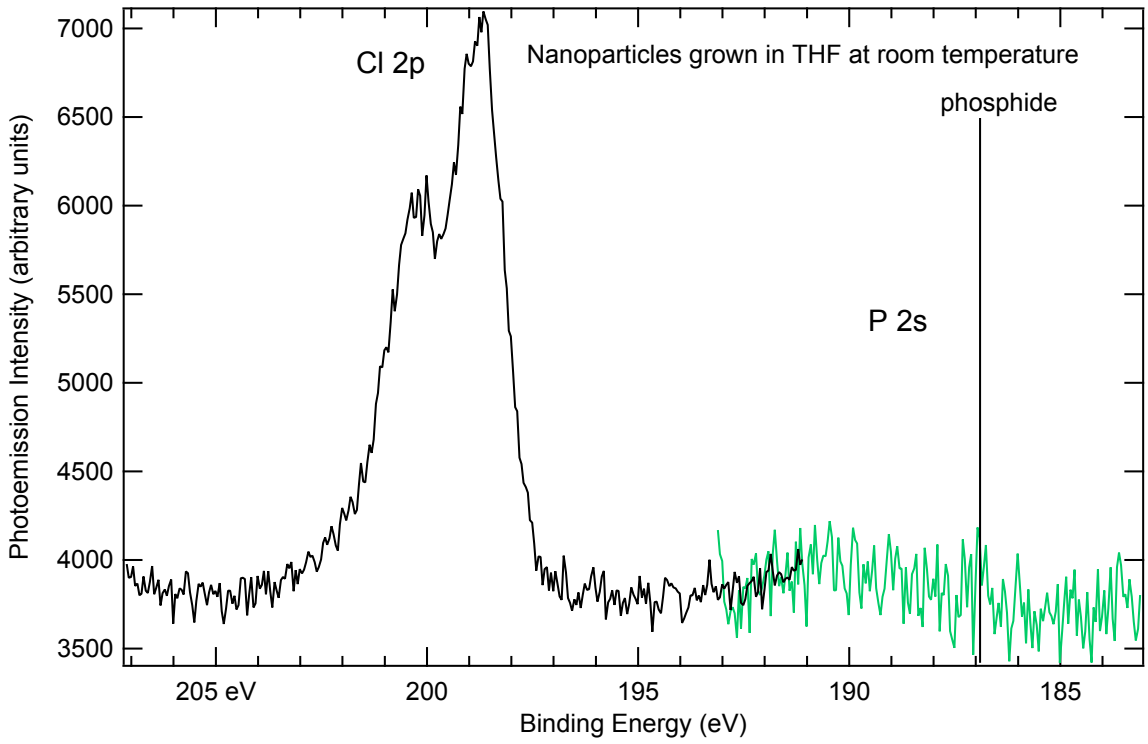

Figure S8. Cl 2p and P 2s spectra of concentrated nanoparticles grown in THF at room temperature. BE are referenced to C 1s positioned at 285.0 eV. A monochromatized Al K_α source (1486.71 eV) was used.

S6. O 1s spectra of concentrated nanoparticles films (spheres, spheres-and-rods, and rods)

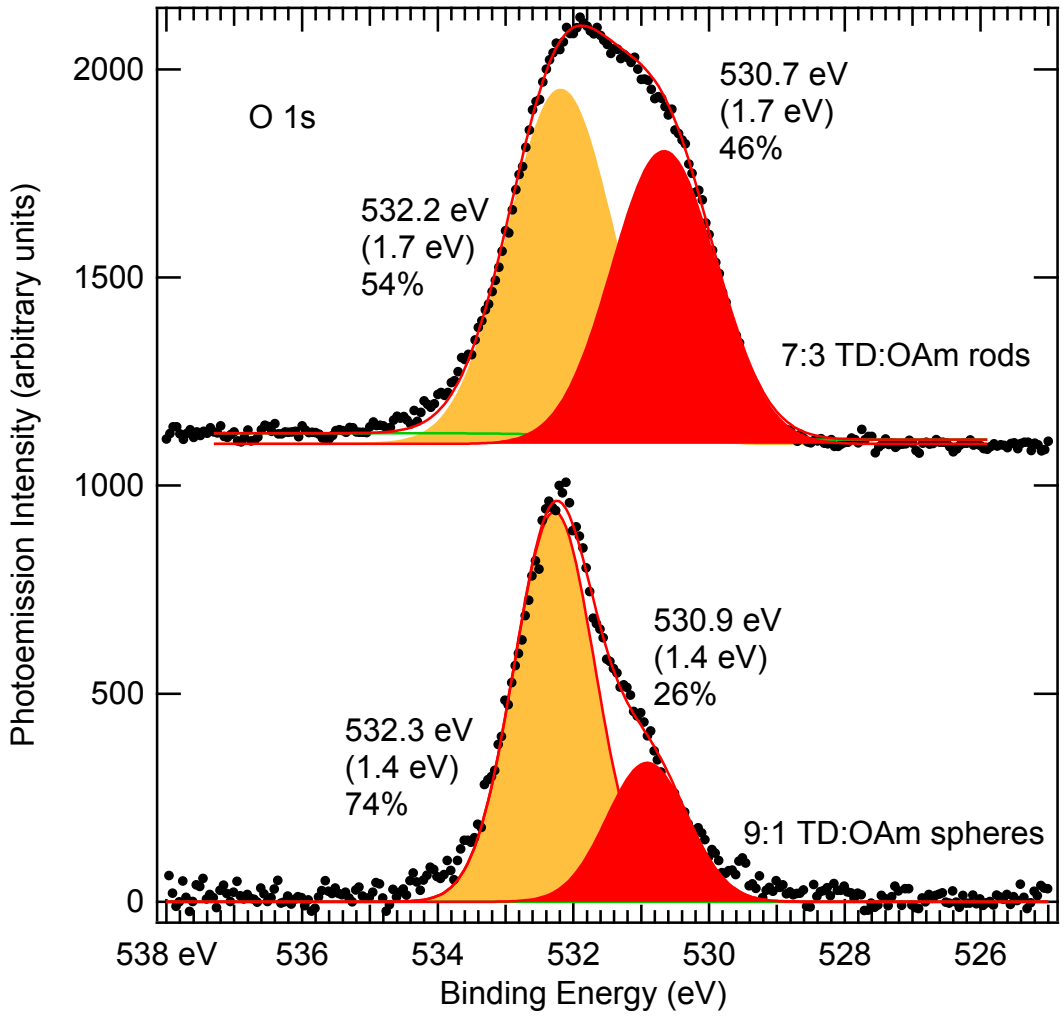

Figure S9. O 1s spectra of concentrated nanoparticles films (spheres, spheres-and-rods, and rods) prepared from centrifugated TD:OAm solutions (the ratio is indicated). BE are referenced to C 1s positioned at 285.0 eV. A monochromatized Al K_α source (1486.71 eV) was used. The experimental curves are fitted with sums of Gaussians (red solid curves), whose BE positions, FWHMs (between parentheses) and spectral weights are also given.

S7. Simulation of cobalt core-level photoemission intensities for OAm-dressed nanoparticles

Nanoparticles are assumed to be cubes of edge D. The cube centers are positioned on a plane square lattice of edge L (L>D). All top cube faces are perpendicular to the detection direction of the photoelectrons. The parallel planes are distant by L. Cubes from different planes are not necessarily aligned vertically. Each metallic cube is covered by an organic layer of thickness $h = (L - D)/2$.

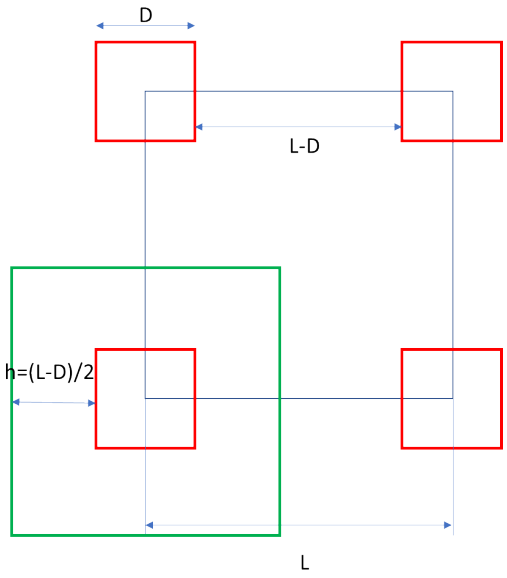

Figure S10. Top view of plane 1.

We consider the cobalt photoemission intensity from plane 1. It is:

$$I_{Co\,CL}(plane\ 1) = K\sigma_{Co\,Cl} n_{Co}^{metal} T_{lens} \lambda_{Co\,CL}^{metal} \left(\frac{D}{L}\right)^2 \left(1 - \exp\left(-\frac{D}{\lambda_{Co\,CL}^{metal}}\right)\right) \exp\left(-\left(\frac{L-D}{2 \times \lambda_{Co\,CL}^{orga}}\right)\right)$$

Below plane 1, we must calculate an average inelastic mean free path $\lambda_{Co\,CL}^{average}$ as the material is inhomogeneous (and cubes are not aligned vertically). Considering the inelastic scattering

probabilities in the metal and in the organic matter as two disjoint events, then $\lambda_{Co\,CL}^{average}$ can be defined as:

$$\frac{1}{\lambda_{Co\,CL}^{average}} = \left(\frac{D}{L}\right)^3 \frac{1}{\lambda_{Co\,CL}^{metal}} + \left(1 - \left(\frac{D}{L}\right)^3\right) \frac{1}{\lambda_{Co\,CL}^{orga}}$$

The intensity of plane 2 (situated at a distance L below) is

$$I_{Co\,CL}(plane\ 2) = I_{Co\,CL}(plane\ 1) \times \exp\left(-\frac{L}{\lambda_{Co\,CL}^{average}}\right)$$

That of plane *n* (situated at a distance $(n-1)L$ below plane 1 is:

$$I_{Co\,CL}(plane\ n) = I_{Co\,CL}(plane\ 1) \times \left(\exp\left(-\frac{L}{\lambda_{Co\,CL}^{average}}\right)\right)^{n-1}$$

The summed contribution of plane 1, plane 2, … plane ∞ (a geometric series of reason $q = \exp\left(-\frac{L}{\lambda_{Co\,CL}^{average}}\right)$) is:

$$I_{Co\,CL} = K\sigma_{Co\,Cl} n_{Co}^{metal} T_{lens} \lambda_{Co\,CL}^{metal} \left(\frac{D}{L}\right)^2 \left(\frac{\left(1 - \exp\left(-\frac{D}{\lambda_{Co\,CL}^{metal}}\right)\right) \exp\left(-\frac{L-D}{2 \times \lambda_{Co\,CL}^{orga}}\right)}{1 - \exp\left(-\frac{L}{\lambda_{Co\,CL}^{average}}\right)}\right)$$

Considering the definitions of $I_{Co\,3p}^{norm}$ and $I_{Co\,2p}^{norm}$

$$\frac{I_{Co\,3p}^{norm}}{I_{Co\,2p}^{norm}} = \frac{\frac{\left(1 - \exp\left(-\frac{D}{\lambda_{Co\,3p}^{metal}}\right)\right) \exp\left(-\frac{L-D}{2 \times \lambda_{Co\,3p}^{orga}}\right)}{1 - \exp\left(-\frac{L}{\lambda_{Co\,3p}^{average}}\right)}}{\frac{\left(1 - \exp\left(-\frac{D}{\lambda_{Co\,2p}^{metal}}\right)\right) \exp\left(-\frac{L-D}{2 \times \lambda_{Co\,2p}^{orga}}\right)}{1 - \exp\left(-\frac{L}{\lambda_{Co\,2p}^{average}}\right)}}$$

This equation can be rewritten considering that the organic layer evenly coating the cube has a thickness h.

Then $L = D + 2h$ and

$$\frac{I^{norm}_{Co\ 3p}}{I^{norm}_{Co\ 2p}}(D,h) = \frac{\left(1 - \exp\left(-\frac{D}{\lambda^{metal}_{Co\ 3p}}\right)\right)\exp\left(-\frac{h}{\lambda^{orga}_{Co\ 3p}}\right)}{1 - \exp\left(-\frac{D+2h}{\lambda^{average}_{Co\ 3p}}\right)} \Bigg/ \frac{\left(1 - \exp\left(-\frac{D}{\lambda^{metal}_{Co\ 2p}}\right)\right)\exp\left(-\frac{h}{\lambda^{orga}_{Co\ 2p}}\right)}{1 - \exp\left(-\frac{D+2h}{\lambda^{average}_{Co\ 2p}}\right)}$$

with $\frac{1}{\lambda^{average}_{Co\ 3p}} = \left(\frac{D}{D+2h}\right)^3 \frac{1}{\lambda^{metal}_{Co\ 3p}} + \left(1 - \left(\frac{D}{D+2h}\right)^3\right)\frac{1}{\lambda^{orga}_{Co\ 3p}}$

and $\frac{1}{\lambda^{average}_{Co\ 2p}} = \left(\frac{D}{D+2h}\right)^3 \frac{1}{\lambda^{metal}_{Co\ 2p}} + \left(1 - \left(\frac{D}{D+2h}\right)^3\right)\frac{1}{\lambda^{orga}_{Co\ 2p}}$

Note that when $h = 0$, $\frac{I^{norm}_{Co\ 3p}}{I^{norm}_{Co\ 2p}} = 1$ and that $\frac{I^{norm}_{Co\ 3p}}{I^{norm}_{Co\ 2p}}(\infty,h) = \frac{\exp\left(-\frac{h}{\lambda^{orga}_{Co\ 3p}}\right)}{\exp\left(-\frac{h}{\lambda^{orga}_{Co\ 2p}}\right)}$ which is exactly the situation of a semi-infinite Co substrate covered by an organic layer of thickness *h*.

The characteristic "length" of OAm is 2.33 nm. We plot $\frac{I^{norm}_{Co\ 3p}}{I^{norm}_{Co\ 2p}}(D,h)$ as a function of the variable *D* for *h*=2.33 nm (one OAm dressing layer) and *h*= 4.66 nm (two OAm dressing layers). The λ values for Co 3p (Co 2p) electrons in bulk cobalt and OAm are 2.1 (1.2) and 3.9 (2.2) nm, respectively. The situation is little affected for the cobalt phosphides, given that their λ's are close to those of Co.

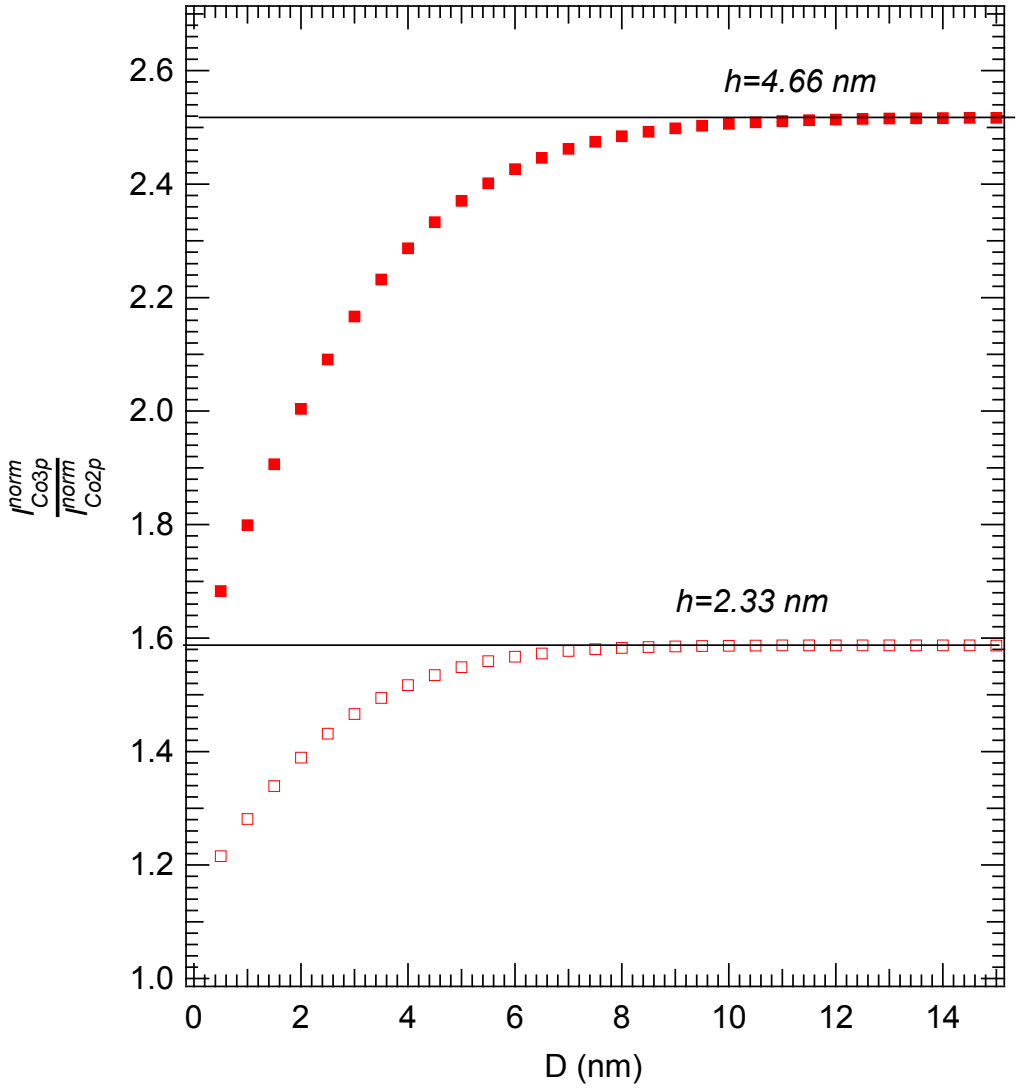

Figure S11. The ratio $\frac{I^{norm}_{Co\ 3p}}{I^{norm}_{Co\ 2p}}(D,h)$ *for two values of h, 2.33 nm (one OAm layer) and 4.66 nm (two OAm layers).*

For *h*=2.33 nm, $\frac{I^{norm}_{Co\ 3p}}{I^{norm}_{Co\ 2p}}(D,h)$ is practically equal to 1.59 when $D > 7$ nm. For *h*=4.66 nm, a limit of 2.6 is attained for $D > 9$ nm. This is exactly the situation of a semi-infinite Co substrate covered by an organic layer of thickness *h in which case the ratio* $\frac{I^{norm}_{Co\ 3p}}{I^{norm}_{Co\ 2p}} = \frac{\exp\left(-\frac{h}{\lambda^{orga}_{Co\ 3p}}\right)}{\exp\left(-\frac{h}{\lambda^{orga}_{Co\ 2p}}\right)}$.

References

(1) Tanuma, S.; Powell, C. J.; Penn, D. R. Calculations of Electorn Inelastic Mean Free Paths. II. Data for 27 Elements over the 50-2000 EV Range. *Surf. Interface Anal.* **1991**, *17* (13), 911–926. https://doi.org/10.1002/sia.740171304.

(2) Tanuma, S.; Powell, C. J.; Penn, D. R. Calculations of Electron Inelastic Mean Free Paths (IMFPS). IV. Evaluation of Calculated IMFPs and of the Predictive IMFP Formula TPP-2 for Electron Energies between 50 and 2000 EV. *Surf. Interface Anal.* **1993**, *20* (1), 77–89. https://doi.org/10.1002/sia.740200112.

(3) Tanuma, S.; Powell, C. J.; Penn, D. R. Calculations of Electron Inelastic Mean Free Paths. V. Data for 14 Organic Compounds over the 50-2000 EV Range. *Surf. Interface Anal.* **1994**, *21* (3), 165–176. https://doi.org/10.1002/sia.740210302.

(4) Tanuma, S.; Powell, C. J.; Penn, D. R. Calculation of Electron Inelastic Mean Free Paths (IMFPs) VII. Reliability of the TPP-2M IMFP Predictive Equation. *Surf. Interface Anal.* **2003**, *35* (3), 268–275. https://doi.org/10.1002/sia.1526.

(5) Tanuma, S.; Powell, C. J.; Penn, D. R. Calculations of Electron Inelastic Mean Free Paths. *Surf. Interface Anal.* **2005**, *37* (1), 1–14. https://doi.org/10.1002/sia.1997.

(6) Powell, C. J.; Jablonski, A. NIST Electron Inelastic-Mean-Free-Path Database, NIST Standard Reference Database 71 Version 1.2. *Gaithersburg* **2010**.

(7) Costner, E. A.; Long, B. K.; Navar, C.; Jockusch, S.; Lei, X.; Zimmerman, P.; Campion, A.; Turro, N. J.; Willson, C. G. Fundamental Optical Properties of Linear and Cyclic Alkanes: VUV Absorbance and Index of Refraction. *J. Phys. Chem. A* **2009**, *113* (33), 9337–9347. https://doi.org/10.1021/jp903435c.

(8) Shard, A. G. Practical Guides for X-Ray Photoelectron Spectroscopy: Quantitative

XPS. *J. Vac. Sci. Technol. A* **2020**, *38* (4), 041201. https://doi.org/10.1116/1.5141395.

(9) Yeh, J. J.; Lindau, I. Atomic Subshell Photoionization Cross Sections and Asymmetry Parameters: 1 < Z <103. *At. Data Nucl. Data Tables* **1985**, *32*, 1–155.

(10) Titus, D. D.; Orio, A. A.; Marsh, R. E.; Gray, H. B. The Crystal and Molecular Structure of Hydridotetrakis(Diethyl Phenylphosphonite)Cobalt(I). *J. Chem. Soc. D Chem. Commun.* **1971**, No. 7, 322. https://doi.org/10.1039/c29710000322.

(11) Choi, H.; Park, S. Liquid Cobalt (I) Hydride Complexes as Precursors for Chemical Vapor Deposition. *Chem. Mater.* **2003**, *15* (16), 3121–3124. https://doi.org/10.1021/cm030100e.

(12) Krzystek, J.; Ozarowski, A.; Zvyagin, S. A.; Telser, J. High Spin Co(I): High-Frequency and -Field EPR Spectroscopy of CoX(PPh 3) 3 (X = Cl, Br). *Inorg. Chem.* **2012**, *51* (9), 4954–4964. https://doi.org/10.1021/ic202185x.

(13) Zhang, X.; Ogitsu, T.; Wood, B. C.; Pham, T. A.; Ptasinska, S. Oxidation-Induced Polymerization of InP Surface and Implications for Optoelectronic Applications. *J. Phys. Chem. C* **2019**, *123* (51), 30893–30902. https://doi.org/10.1021/acs.jpcc.9b07260.

(14) Zakhtser, A.; Naitabdi, A.; Benbalagh, R.; Rochet, F.; Salzemann, C.; Petit, C.; Giorgio, S. Chemical Evolution of Pt–Zn Nanoalloys Dressed in Oleylamine. *ACS Nano* **2021**, *15* (3), 4018–4033. https://doi.org/10.1021/acsnano.0c03366.